

Copyright
by
Robert Clark Daniels
2006

**An M-ary Continuous Phase Modulated System with
Coherent Detection and Frequency Domain
Equalization**

by

Robert Clark Daniels, B.S.

REPORT

Presented to the Faculty of the Graduate School of
The University of Texas at Austin
in Partial Fulfillment
of the Requirements
for the Degree of

MASTER OF SCIENCE IN ENGINEERING

THE UNIVERSITY OF TEXAS AT AUSTIN

May 2006

**An M-ary Continuous Phase Modulated System with
Coherent Detection and Frequency Domain
Equalization**

APPROVED BY

SUPERVISING COMMITTEE:

Robert W. Heath, Jr., Supervisor

Jeffrey Andrews

Dedicated to my family.

An M -ary Continuous Phase Modulated System with Coherent Detection and Frequency Domain Equalization

Robert Clark Daniels, M.S.E.
The University of Texas at Austin, 2006

Supervisor: Robert W. Heath, Jr.

Continuous phase modulation (CPM) for wireless communications is a method of constant envelope (CE) signal transmission where the information bearing portion of the signal is encoded continuously in the phase. While CPM exhibits power efficient transmission, it suffers from increased complexity in the receiver design. Moreover, CPM has largely been analyzed using the narrowband channel assumption. That is, the wireless channel is assumed frequency flat with no intersymbol interference (ISI). This assumption has limited the application of CPM techniques in current wireless technologies such as wireless local area and personal area networks (WLANs and WPANs). In this report we develop a CPM system enabled by Laurent's [13] decomposition method for binary CPM signals extended by Mengali and Morelli [14] to M -ary modulations. We apply frequency domain equalization, where, similar to OFDM, equalization is performed in the frequency domain. This allows us

to derive a low-complexity coherent receiver for CPM in frequency selective wireless channels. Others have considered the implementation of CPM with frequency domain equalization [21] [16], but none have used the Mengali and Morelli decomposition with traditional transmitter design for M-ary signals.

Table of Contents

| | |
|---|-----------|
| Abstract | v |
| Chapter 1. Introduction | 1 |
| Chapter 2. System Description | 5 |
| 2.0.1 Transmitter | 5 |
| 2.0.2 Receiver | 7 |
| Chapter 3. CPM Decomposition | 9 |
| 3.0.3 Full Decomposition | 9 |
| 3.0.4 Approximate Decomposition | 12 |
| Chapter 4. Receiver Design | 15 |
| 4.0.5 Receiver Filtering and Digital Representation | 16 |
| 4.0.5.1 AWGN Channel | 16 |
| 4.0.5.2 Frequency Selective Channel | 18 |
| 4.0.6 DFT Operation | 19 |
| 4.0.6.1 Continuous Phase Structure | 20 |
| 4.0.6.2 Zero Prefix Structure | 22 |
| 4.0.7 MMSE-LE FDE | 23 |
| 4.0.8 Complexity Discussion | 25 |
| Chapter 5. Conclusion | 28 |
| Bibliography | 29 |
| Vita | 32 |

Chapter 1

Introduction

Modern wireless system implementations result from tradeoffs made between a multitude of system parameters. One such parameter is system power efficiency. System power efficiency is primarily considered on three different layers of the communication system: (1) Physical (2) Link (3) Network. This report will be concerned with power efficiency in the context of the physical and link layers. In particular, we focus on power efficiency as it relates to radio-frequency (RF) hardware design and power consumption by the modulation strategy of the communication system.

Linearly modulated communication systems, such as quadrature amplitude modulation (QAM), require linear operation of power amplifiers (PAs). Practical PAs, however, operate linearly in regions below maximum output power [5]. That is, not only does clipping exist, but non-linear amplification also occurs in the upper region of the input/output voltage curve. Thus, to avoid non-linear distortion in the modulation, PAs must be operated in regions below the maximum power output or saturation point. Additionally, in general, linearly operating amplifiers are more expensive. Therefore, if modulation design can tolerate the nonlinearity of PAs, lower cost transmitter

designs result.

The above discussion motivates modulation techniques that allow PAs to operate in the nonlinear saturation region. Constant envelope modulation (CEM) is a generalized modulation technique where all of the information bearing portion of the transmitted signal is stored in the phase [19]. Therefore, PAs may saturate while a phase modulator encodes the information into the transmitted signal. A more specific (and more recognized) CEM technique is continuous-phase modulation (CPM). Continuous-phase modulation, as the name suggests, restricts CEM waveforms to the specific case where the phase modulation is performed continuously [1]. In other words, the phase of the CPM signal is a continuous function of time. Restricting our CEM system to continuous-phase makes for simpler designs as well as higher bandwidth efficiency in the transmitter. Rapid fluctuations in phase lead to spectral spreading, increasing bandwidth and hardware complexity.

Drawbacks of CPM systems are two-fold. First, CPM systems suffer from lower system capacity when compared to linear modulation [22]. Second, CPM suffers from increased complexity in receiver designs [4], [10]. Because the phase is held continuous, memory is introduced into the phase. This means that symbol by symbol detectors are not able to be used for the general CPM system. Additionally, since phase changes will likely occur within symbol periods, analog filter banks are present. Indeed, effective methods of sampling and processing received CPM signals is a subject of much research. Several authors have provided signal decomposition methods for CPM signals (see [13], [14],

[17] for example). The aforementioned decomposition methods provide a basis representation. Using a filter bank matched to the basis signals it is possible to obtain discrete values for each transmitted symbol. Particularly effective full and approximate decomposition techniques were provided by Laurent [13] such that relatively few basis functions accurately define each transmitted symbol.

Most have assumed CPM signals transmitted in frequency flat environments. If, however, we consider frequency selective wireless channels, equalization methods must be performed on the discrete signal samples. Many current wireless systems implement orthogonal frequency division multiplexing (OFDM) to mitigate high delay spreads caused by a rich wireless environment and/or large bandwidths. Some have considered a combination of OFDM and CPM, however, none have been able to maintain the phase continuity and nonlinear immunity at the actual transmitter. As a result, Tan and Stuber in [21] considered single carrier frequency domain equalization (SC-FDE) in concert with CPM signals. Frequency domain equalization (FDE) is able to reduce the equalizer complexity like OFDM by using the FFT algorithm at the receiver. Both methods perform similarly (in fact they perform almost identically) [5], however, SC-FDE does suffer from a reduced spectral efficiency. Alternatively, OFDM suffers from a large peak-to-average power ratio (PAPR) further motivating FDE.

In this report, as in [21], we consider SC-FDE with CPM. In [21] the receiver and frequency domain equalizer were constructed using a simple orthogonal basis for the M-ary CPM signals derived from the tilted phase trellis

[17]. For binary CPM signals, Laurent's decomposition method was also considered. Here we shall consider implementing SC-FDE for M-ary CPM systems using a generalization of Laurent's decomposition developed by Mengali and Morelli [14]. This decomposition method results in lower complexity receiver implementations for general M-ary CPM signals. The implementation was also investigated in [16], however the authors did not consider traditional transmitter designs, limiting the direct application of the results.

The organization of this report is as follows. Chapter 2 previews the CPM system to be studied. The next chapter, Chapter 3, provides the general M-ary CPM decomposition framework derived from [14]. Chapter 4 presents FDE following the signal decomposition. Finally, Chapter 5 concludes this report and discusses future research directions. Capital letters A will denote fixed integers, bold capital letters \mathbf{A} will denote matrices, $(\bullet)^T$ denotes matrix transpose, \mathbb{Q} is the field of rational numbers, \mathbb{R} is the field of real numbers, \mathbb{C} is the field of complex numbers, $\mathbb{N} = \{1, 2, \dots\}$ is the set of natural numbers, $j = \sqrt{-1}$, \star is the continuous-time convolution operator, $\Re(\bullet)$ denotes the real part, $\lfloor \bullet \rfloor$ denotes the floor function, and $(\bullet)^*$ denotes complex element conjugation. We represent a sequence with index k from A to B as $\{\bullet\}_{k=A}^B$.

Chapter 2

System Description

Figure 2.1 summarizes the system description for the general M -ary CPM system with FDE. We begin discussion with the general transmitter design followed by the general receiver scheme. Some functions such as prefix addition/removal and phase flushing (to be discussed later) are not included in this figure to maintain simplicity.

2.0.1 Transmitter

We consider block transmission of the input bitstream $\{x_k\}_{k=0}^{NK-1}$ where $x_k \in \{0, 1\}$ and k denotes the bit index. Next, the input bitstream is converted to M -ary data symbols. We will assume in this paper that M is a power of 2. This assumption is not a restriction, it is just used for clarity as the analysis presented here does extend to any integer. In other words, $M = 2^K$ where K is the number of bits represented by each data symbol. Therefore the M -ary converter buffers K bits before converting to the data symbol α_n . Specifically $\{x_k, x_{k+1}, \dots, x_{k+K-1}\}$ is mapped to α_n where $n = \frac{k}{K}$ for $k \in \{0, K, 2K, \dots, (N-1)K\}$ and $\alpha_n \in \{\pm 1, \pm 3, \dots, \pm(M-3), \pm(M-1)\}$. Thus we transmit NK -length bit blocks and N -length data blocks.

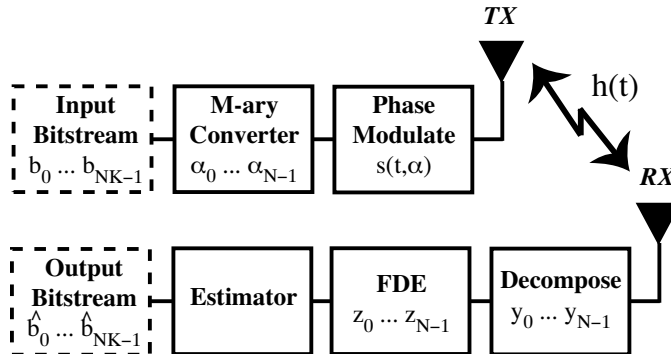


Figure 2.1: M-ary CPM with FDE system model

Next we define the excess phase function to characterize the phase of the CPM transmitted signal as a function of time, t ,

$$\psi(t, \boldsymbol{\alpha}) \triangleq 2\pi h \sum_{n=0}^{N-1} \alpha_n q(t - nT_s) \quad (2.1)$$

where

$$\boldsymbol{\alpha} \triangleq [\alpha_0, \alpha_1, \dots, \alpha_{N-1}]^T, \quad (2.2)$$

h is the modulation index, T_s is the intersymbol time, and $q(t)$ is the phase pulse as a function of time. This method of characterizing the phase of the CPM signal was pioneered by Aulin and Sundberg in [3], [2]. The modulation index

$$h = \frac{u}{v} \in \mathbb{Q} \quad (2.3)$$

where u and v co-prime integers and the phase pulse $q(t) : \mathbb{R} \rightarrow \mathbb{R}$ are both standard in this CPM definition. Integer modulation indexes for h have also been considered, but is not included in this paper [9]. The phase pulse $q(t)$

can be defined in terms of the frequency pulse

$$q(t) = \int_{-\infty}^t g(\tau) d\tau. \quad (2.4)$$

The frequency pulse is standardly defined as

$$g(t) = \begin{cases} 0 & t < 0, t > LT_s \\ \text{nonzero} & 0 \leq t \leq LT_s \end{cases} \quad (2.5)$$

for integer L . If $L = 1$ the system is full response and if $L \in \{\mathbb{N} \setminus 1\}$ the system is partial response. Additionally we constrain $q(t) = \frac{1}{2}$ for $t > LT_s$ such that the energy in the frequency pulse is normalized.

The modulated signal is transmitted over a wireless frequency selective channel. The complex baseband equivalent transmitted signal is

$$s(t, \boldsymbol{\alpha}) \triangleq e^{j\psi(t, \boldsymbol{\alpha})} \quad (2.6)$$

which is, in general, complex. Next we define the complex baseband equivalent channel as $h(t) : \mathbb{R} \rightarrow \mathbb{C}$. It should be noted that $h(t)$ represents a physically feasible, causal, complex baseband frequency selective channel implying $h(t) = 0$ for $t < 0$ and the nonzero amplitude duration of $h(t)$ is greater than the symbol time T_s .

2.0.2 Receiver

After transmission through the channel the received signal is represented by

$$r(t, \boldsymbol{\alpha}) = s(t, \boldsymbol{\alpha}) \star h(t) + v(t) \quad (2.7)$$

where $v(t)$ is a zero mean complex Gaussian noise process such that

$$\mathbb{E}[v(t)v^*(t')] = \begin{cases} 0 & t \neq t' \\ \sigma^2 & t = t' \end{cases} \quad (2.8)$$

with the real and imaginary components as independent zero mean Gaussian random processes parameterized by variance $\sigma^2/2$. The received signal is decomposed into a vector \mathbf{y}_n of discrete components through a series of matched filters for each index n every T_s seconds. This N -length stream of discrete vectors is then processed through an FDE yielding \mathbf{z}_n as the equalized discrete version of the CPM signal. This vector \mathbf{z}_n is then mapped back into the M -ary data symbol $\hat{\alpha}_n$ and finally to the output bitstream \hat{x}_k .

Chapter 3

CPM Decomposition

In 1986, Laurent included a decomposition method for binary full and partial response CPM systems. The derivation of this decomposition is not included in this paper, but the reader is encouraged to observe [13] and the excellent supplementary derivation in [8]. In this section we present the results from Mengali and Morelli [14] which extend Laurent's work to M -ary full and partial response CPM systems. Additionally we detail approximate decomposition to further reduce complexity in the CPM receiver. In Chapter 4 we will use this decomposition to provide basis functions for our matched filter bank as well as enable frequency domain equalization (FDE) in the coherent receiver design.

3.0.3 Full Decomposition

Laurent's decomposition of binary full and partial response CPM systems shows that any binary CPM signal can be represented as a complex linear combination of time-pulse functions named Laurent functions. Specifically, the transmitted binary CPM signal, $s(t, \boldsymbol{\alpha})$ where $\alpha_n \in \{-1, 1\}$, may be written

as

$$\begin{aligned} s(t, \boldsymbol{\alpha}) &= e^{j\psi(t, \boldsymbol{\alpha})} \\ &= \sum_{n=0}^{N-1} \sum_{l=0}^{Q-1} c_l[n] d_l(t - nT_s) \end{aligned} \quad (3.1)$$

for

$$Q = 2^{L-1}, \quad (3.2)$$

$$c_l[n] = \exp \left\{ jh\pi \left[\sum_{m=-\infty}^n \alpha_m - \sum_{i=0}^{L-1} \alpha_{n-i} \beta_l[i] \right] \right\}, \quad (3.3)$$

$$d_l(t) = \prod_{i=0}^{L-1} u(t + iT_s + \beta_l[i] LT_s), \quad (3.4)$$

$$u(t) = \begin{cases} \frac{\sin(2h\pi q(t))}{\sin(h\pi)} & 0 \leq t \leq LT_s \\ \frac{\sin(2h\pi q(2LT_s - t))}{\sin(h\pi)} & LT_s < t \leq 2LT_s \\ 0 & \text{otherwise} \end{cases}, \quad (3.5)$$

where

$$0 \leq l \leq Q - 1 \quad (3.6)$$

and $\beta_l[i] \in \{0, 1\}$ such that $\beta_l[0] = 0$ with $\beta_l[i]$ representing the i th bit in the modulo-2 value of l , i.e.

$$l = \sum_{i=1}^{L-1} 2^{i-1} \beta_l[i]. \quad (3.7)$$

It should be noted that, although this decomposition does not lend much obvious intuitive insight into the nature of CPM signals, it is an invaluable tool for creating discrete representations of the signal at the receiver. By correlating the signal with the $Q = 2^{L-1}$ distinct time-pulse functions $d_l(t)$ we receive the discrete Q -dimensional signal representation every T_s seconds. Further explanation of this topic will be covered in Section 4.0.5.

The above binary decomposition method was generalized to M -ary signals in [14] as follows. Recalling that $M = 2^K$ define

$$\tilde{\alpha}_n \triangleq \frac{\alpha_n + 2^K - 1}{2} \Rightarrow 0 \leq \tilde{\alpha}_n \leq 2^K - 1 \quad (3.8)$$

$$\Leftrightarrow 0 \leq \tilde{\alpha}_n \leq M - 1 \quad (3.9)$$

$$\Rightarrow \tilde{\alpha}_n = \sum_{m=0}^{K-1} \tilde{\gamma}_n[m] 2^m \quad (3.10)$$

where $\tilde{\gamma}_n[m] \in \{0, 1\}$ in (3.10). It follows from (3.8) that α_n may be represented as

$$\alpha_n = 2 \sum_{m=0}^{K-1} \tilde{\alpha}_n 2^m - (M - 1) \quad (3.11)$$

$$= 2 \sum_{m=0}^{K-1} \tilde{\alpha}_n 2^m - \sum_{m=0}^{K-1} 2^m \quad (3.12)$$

$$= 2 \sum_{m=0}^{K-1} 2^m \left(\tilde{\gamma}_n[m] - \frac{1}{2} \right) \quad (3.13)$$

$$= \sum_{m=0}^{K-1} 2^m \gamma_n[m] \quad (3.14)$$

given that $\gamma_n[m] \triangleq 2 \left(\tilde{\gamma}_n[m] - \frac{1}{2} \right)$. Thus $\gamma_n[m] \in \{-1, 1\}$. Combining (3.14) with (2.6) we obtain

$$s(t, \boldsymbol{\alpha}) = \exp \left\{ j2\pi h \sum_{n=0}^{N-1} \sum_{m=0}^{K-1} 2^m \gamma_n[m] q(t - nT_s) \right\} \quad (3.15)$$

$$= \exp \left\{ j2\pi h \sum_{m=0}^{K-1} 2^m \sum_{n=0}^{N-1} \gamma_n[m] q(t - nT_s) \right\} \quad (3.16)$$

$$= \prod_{m=0}^{K-1} \exp \left\{ j2\pi h 2^m \sum_{n=0}^{N-1} \gamma_n[m] q(t - nT_s) \right\} \quad (3.17)$$

$$= \prod_{m=0}^{K-1} \exp \left\{ j2\pi h^{(m)} \sum_{n=0}^{N-1} \gamma_n[m] q(t - nT_s) \right\} \quad (3.18)$$

where $h^{(m)} \triangleq h2^m$. Thus, (3.18) shows that any M -ary full or partial response CPM signal may be represented as a product of K binary CPM signals. Therefore, we can approach the M -ary case in much the same fashion as in [13].

Let the superscript $(\bullet)^{(m)}$ denote the decomposition component associated with the m th product in (3.18). Utilizing Laurent's decomposition we have

$$s(t, \boldsymbol{\alpha}) = \prod_{m=0}^{K-1} \sum_{n=0}^{N-1} \sum_{l=0}^{Q-1} c_l [n]^{(m)} d_l^{(m)}(t - nT_s). \quad (3.19)$$

Although we have demonstrated that the M -ary CPM signal may be decomposed into a product of a linear combination of time phase pulses, this doesn't necessarily facilitate receiver design. Observe that we could easily derive a representation resulting in a sum of $(Q \times N)^K$ pulses by simply extracting the individual terms in (3.19). Mengali and Morelli detailed a reduced decomposition, in fact, where they showed that

$$s(t, \boldsymbol{\alpha}) = \sum_{l=0}^{P-1} \sum_{n=0}^{N-1} a_l [n] b_l(t - nT_s) \quad (3.20)$$

with $P = Q^K \times (M - 1)$. The actual computation of $a_{l,n}$ and Laurent function $b_l(t)$ is tedious and does not lend much insight. For this reason it is not included here. The reader is encouraged to reference [14] for completeness.

3.0.4 Approximate Decomposition

The decomposition given in (3.20) and detailed in Section 3.0.3 gives an exact representation of the CPM signal in terms of a sum of amplitude modulated Laurent functions. An unstated characteristic of these Laurent functions

(or time-pulses) is that each pulse does not contain an equal contribution in the CPM signal $s(t, \boldsymbol{\alpha})$. Therefore, one simple approximation of the CPM signal $s(t, \boldsymbol{\alpha})$ is to only consider the Laurent functions $b_l(t)$ in (3.20) containing the most energy. It has been experimentally observed that most of the energy is contained within the first $M - 1$ Laurent functions. This approximation, however, is not optimal in terms of minimum mean square error (MMSE). In fact, [14] presented a procedure to construct MMSE optimal pulses, $\hat{b}_l(t)$, that are amplitude modulated by $a_{l,n}$. This process is more precisely specified below.

Given the complete decomposition in (3.20) we construct R MMSE pulses $\hat{b}_l(t), l \in \{1, 2, \dots, R\}$ for

$$\hat{s}(t, \boldsymbol{\alpha}) = \sum_{l=0}^{R-1} \sum_{n=0}^{N-1} a_l[n] \hat{b}_l(t - nT_s) \quad (3.21)$$

such that

$$\left\{ \hat{b}_l(t) \right\}_{l=1}^R = \arg \min_{\left\{ \hat{b}_l(t) \right\}_{l=1}^R} \left\{ \frac{1}{T} \int_0^{T_s} \mathbb{E} \left\{ |s(t, \boldsymbol{\alpha}) - \hat{s}(t, \boldsymbol{\alpha})|^2 \right\} dt \right\} \quad (3.22)$$

$$= \arg \min_{\left\{ \hat{b}_l(t) \right\}_{l=1}^R} \left\{ \mathbb{E} \left\{ |s(t, \boldsymbol{\alpha}) - \hat{s}(t, \boldsymbol{\alpha})|^2 \right\} \forall t \in [0, T_s] \right\}. \quad (3.23)$$

Laurent [13] showed that by taking the derivative of (3.23) and setting it equal to zero we are able to state

$$\sum_{i=0}^{R-1} \sum_{n=0}^{N-1} r_{a_{l,i}}[m-n] \hat{b}_i(t + nT_s) = \sum_{i=0}^{P-1} \sum_{n=0}^{N-1} r_{a_{l,i}}[m-n] b_i(t + nT_s) \quad (3.24)$$

for MMSE optimal pulses given $r_{a_{l,i}}[m] \triangleq \mathbb{E} \{ a_l[n] a_i^*[n+m] \}$. Notice the terms in the summations of equation (3.24) are discrete-time convolutions

implying the equivalent statement

$$\sum_{i=0}^{R-1} \mathcal{R}_{a_{l,i}}(f) \hat{B}_i(f) = \sum_{i=0}^{P-1} \mathcal{R}_{a_{l,i}}(f) B_i(f) \quad (3.25)$$

where $\mathcal{R}_{a_{l,i}}(f)$, $B(f)$, $\hat{B}(f)$ are the discrete-time Fourier transforms (DTFT) of $r_{a_{l,i}}[n]$, $b_i(t + nT_s)$, $\hat{b}_i(t + nT_s)$ respectively. If we let

$$\mathbf{A}(f) \triangleq \begin{bmatrix} \mathcal{R}_{a_{0,0}} & \cdots & \mathcal{R}_{a_{0,R-1}} \\ \vdots & \ddots & \vdots \\ \mathcal{R}_{a_{R-1,0}} & \cdots & \mathcal{R}_{a_{R-1,R-1}} \end{bmatrix}, \quad (3.26)$$

$$\tilde{\mathbf{A}}(f) \triangleq \begin{bmatrix} \mathcal{R}_{a_{0,R}} & \cdots & \mathcal{R}_{a_{0,P-1}} \\ \vdots & \ddots & \vdots \\ \mathcal{R}_{a_{R-1,0}} & \cdots & \mathcal{R}_{a_{R-1,P-1}} \end{bmatrix}, \quad (3.27)$$

$$\mathbf{B}(f) \triangleq [B_0(f) \cdots B_{R-1}(f)]^T, \quad (3.28)$$

$$\hat{\mathbf{B}}(f) \triangleq [\hat{B}_0(f) \cdots \hat{B}_{R-1}(f)]^T, \quad (3.29)$$

we see that

$$\hat{\mathbf{B}}(f) = \mathbf{A}^{-1}(f) \tilde{\mathbf{A}}(f) \mathbf{B}(f) + \mathbf{B}(f). \quad (3.30)$$

Taking the inverse discrete-time Fourier transform (IDTFT) of (3.30) it can be shown that

$$\hat{b}_l(t) = b_l(t) + \sum_{i=R}^{P-1} \sum_{n=0}^{P-1} \lambda_{l,i}[n] b_l(t - nT_s) \quad (3.31)$$

where $\lambda_{l,i}[n] = T_s \int_{-1/2T_s}^{1/2T_s} \Lambda_{l,i}(f) e^{j2\pi n f T_s} df$ for $\Lambda_{l,i}(f) = \tilde{\Lambda}_{l,i-R}(f)$ and

$$\tilde{\mathbf{\Lambda}}(f) \triangleq \begin{bmatrix} \tilde{\Lambda}_{0,R}(f) & \cdots & \tilde{\Lambda}_{0,P-1}(f) \\ \vdots & \ddots & \vdots \\ \tilde{\Lambda}_{R-1,R}(f) & \cdots & \tilde{\Lambda}_{R-1,P-1}(f) \end{bmatrix} \quad (3.32)$$

$$= \mathbf{A}^{-1}(f) \tilde{\mathbf{A}}(f). \quad (3.33)$$

Chapter 4

Receiver Design

With the decomposition method established in Chapter 3 we now proceed with details of the filtering and equalization process. First, we shall describe the channel modification of the digital equivalent transmitted signal. Then we equalize to remove the intersymbol interference effects on the signal. Figure 4.1 summarizes the coherent detection receiver design described in this paper. We will assume perfect phase synchronization in the detection process (see [4] for implementation details).

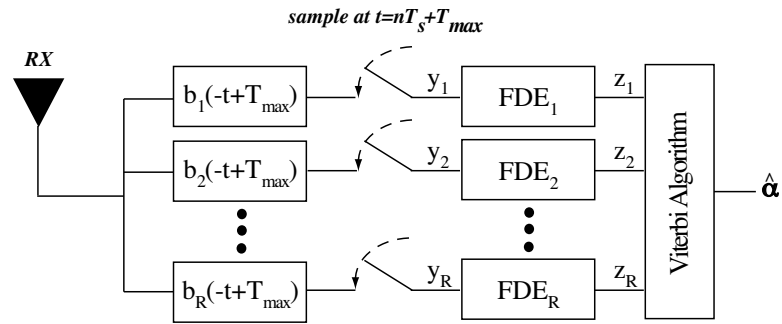


Figure 4.1: Baseband FDE receiver block diagram

4.0.5 Receiver Filtering and Digital Representation

Using (3.20) or (3.21) to represent the transmitted signal we implement P or R matched filters, respectively, to create the discrete version of the received signal. This coherent detection design was first proposed by Kaleh in [12] for binary partial response CPM signaling and extended by Colavolpe and Raheli [4] to the M -ary case. Clearly, this receiver design is independent of whether or not we use the approximated description of the transmitted signal. The only distinction is associated with the number of matched filters used in the receiver. From this point forward we proceed by analyzing the approximate decomposition with the assumption that all analysis directly applies to the full decomposition as well. Before continuing with the analysis for frequency selective channels, we detail the optimal additive white Gaussian noise (AWGN) channel coherent CPM receiver in Figure 4.1 [12]. Then we analyze the frequency selective scenario by implementing frequency domain equalization to eliminate intersymbol interference effects.

4.0.5.1 AWGN Channel

For an AWGN channel ISI effects are absent, eliminating the FDE components in the receiver design. With partial response pulse decomposition (the pulses $\hat{b}_l(t)$ are, in general, partial response even when the CPM system is full response) the successive samples $y_l[n]$ contain information from previous symbols. Thus, one may consider the entire sequence of N M -ary symbols in order to decide the most likely N -length symbol sequence transmitted,

i.e. maximum likelihood sequence estimation (MLSE) [6]. The most obvious (and overly complex) way to obtain the maximum likelihood sequence is to implement M^N matched filters corresponding to each possible transmitted signal representing a N -length M -ary symbol sequence.

Kaleh proposed an alternate MLSE procedure operating on the principles of the Viterbi algorithm [12]. If instead we implement R matched filters corresponding to each MMSE Laurent pulse $\hat{b}_l(t)$ in (3.20) we can calculate a branch metric $\lambda_i[n]$ (a sufficient statistic) for the i th N -length symbol sequence at $t = T_{max} + nT_s$ seconds using the matched filter outputs ($i \in \{1, 2, \dots, M^K\}$). This is the scenario depicted in Figure 4.1. The delay of T_{max} seconds is used to physically realize the anticausal matched-filter impulse responses where $T_{max} \triangleq \max_l \{t : \hat{b}_l(t) \neq 0\}$. Specifically,

$$y_l[n] \triangleq \int_{nT_s}^{nT_s+T_{max}} r(\tau) \hat{b}_l(\tau + T_{max} - t) d\tau \Big|_{t=nT_s+T_{max}} \quad (4.1)$$

$$= \int_{nT_s}^{nT_s+T_{max}} r(\tau) \hat{b}_l(\tau - nT_s) d\tau \quad (4.2)$$

such that

$$\lambda_i[n] \triangleq \Re \left\{ \sum_{l=0}^{P-1} y_l[n] a_{l,n}^{i*} \right\} \quad (4.3)$$

is the branch metric definition for time $t = nT_s$. With this definition the maximum likelihood sequence is chosen as \hat{i} if

$$\hat{i} = \arg \max_i \sum_{n=0}^{N-1} \lambda_i[n]. \quad (4.4)$$

This computational process is simply the VA applied to the outputs of the matched-filters.

4.0.5.2 Frequency Selective Channel

We now extend the work proposed by [12] to frequency selective channels by including FDEs after each matched-filter operation. The matched filter sample is

$$\begin{aligned} y_l[n] &\triangleq \int_{nT_s}^{nT_s+T_{max}} r(\tau) \hat{b}_l(\tau - nT_s) d\tau \\ &= \int_{nT_s}^{nT_s+T_{max}} (s(\tau, \boldsymbol{\alpha}) \star h(\tau) + v(\tau)) \hat{b}_l(\tau - nT_s) d\tau \end{aligned} \quad (4.5)$$

as expanded from (4.2). By invoking the frequency-selective channel model [20] we have

$$h(t) = \sum_{i=0}^{\nu} h[i] \delta(t - iT_s) \quad (4.6)$$

where by substitution in (4.5)

$$y_l[n] = \int_{nT_s}^{nT_s+T_{max}} \left(\sum_{i=0}^{\nu} h[i] s(\tau - iT_s, \boldsymbol{\alpha}) + v(\tau) \right) \hat{b}_l(\tau - nT_s) d\tau \quad (4.7)$$

$$= \sum_{i=0}^{\nu} h[i] \int_{nT_s}^{nT_s+T_{max}} s(\tau - iT_s, \boldsymbol{\alpha}) \hat{b}_l(\tau - nT_s) d\tau + \quad (4.8)$$

$$\int_{nT_s}^{nT_s+T_{max}} v(\tau) \hat{b}_l(\tau - nT_s) d\tau \quad (4.9)$$

$$= \sum_{n=0}^{\nu} h[i] \tilde{y}_l[n - i] + \tilde{v}_l[n] \quad (4.10)$$

represents the matched filter samples for ν taps of delay spread in the frequency selective channel where $\tilde{y}_l[n] \triangleq \int_{nT_s}^{nT_s+T_{max}} s(\tau - nT_s, \boldsymbol{\alpha}) \hat{b}_l(\tau - nT_s) d\tau$ and $\tilde{v}_l[n] \triangleq \int_{nT_s}^{nT_s+T_{max}} v(\tau) \hat{b}_l(\tau - nT_s) d\tau$. Notice that the matched-filter samples are the result of a scaled sum of AWGN samples (with a correlated noise term). We are now in the position to remove ISI effects on the matched filter samples.

4.0.6 DFT Operation

Frequency domain equalization, as the name implies, eliminates intersymbol interference through frequency domain operations. To properly implement the discrete fourier transform (DFT) and enter the frequency domain, we must ensure that the discrete data is cyclic in discrete-time. In other words, the N -length sequence $\{y_l[n]\}_{n=0}^{N-1}$ must be cyclic. This implies that intersymbol interference effects from the tail of the N -length sequence carry over into the beginning of the sequence. Traditionally, in OFDM and single carrier FDE a cyclic prefix of ν symbols consisting of the last ν of N data symbols is placed on the sequence at the transmitter and then removed at the receiver before symbol processing such that the ISI effects are cyclic [7] and separate between data blocks. In the coherent detection scheme detailed in Section 4.1 the matched-filter samples are derived from partial response symbols. Thus, each received symbol period contains information from previous symbols. T_{max} describes the largest Laurent pulse duration. Each received matched filter sample $y_l[n]$ contains information from $(T_{max} - T_s)$ seconds of received signal data before. Therefore if $\eta = \frac{T_{max} - T_s}{T_s}$ then the value of $y_l[n']$ depends on samples $\{y_l[n]\}_{n=n'-\eta}^{n'-1}$. With these dependencies in mind, we develop two scenarios for transmitter symbol structure to enable DFT operation. The first scenario maintains continuous phase by inserting a prefix consisting of the tail symbols which are separated from the main data block by specific data separation symbols. The second scenario involves less overhead by turning off transmission between continuous phase data blocks.

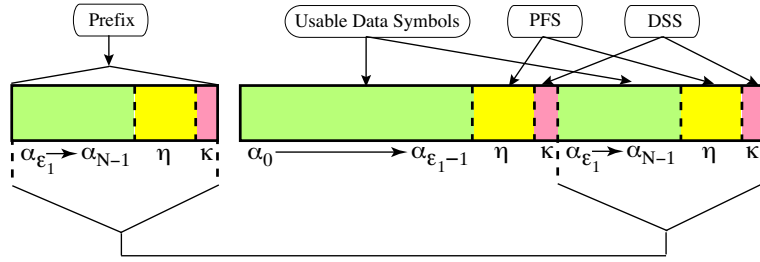


Figure 4.2: Continuous phase transmission data symbol structure

4.0.6.1 Continuous Phase Structure

As discussed above we desire to place a prefix consisting of the last ν data symbols at the transmitter such that the intersymbol interference effects bleed into the beginning of the data block. Unfortunately, the matched-filter symbols $y_l[n]$ depend on η prior symbols. We must ensure that before and after the last ν data symbols we insert η data separation symbols. Additionally, we must maintain continuous phase between data blocks. This implies that the beginning and end of each data block has equivalent phase. Since the data block ends with η data separation symbols, we must maintain phase continuity at several points in the N -length data block. For this report we will assume the beginning and end of each data block are zero phase and that the data separation symbols are known and begin and end with zero phase symbols. Before the first and second data separation symbols we need to return to zero phase. This transmission data block structure is displayed in Figure 4.2 and summarized below:

- Phase Flush Symbols (PFS): Maintaining phase continuity requires re-

turning to zero-phase before the data separation symbols. Moqvist and Aulin detailed an efficient scheme in [15] for phase flushing. Their scheme requires κ PFS where $\kappa = \lfloor \frac{v-1}{M-1} \rfloor + L$ for v in (2.3).

- Data Separation Symbols (DSS): In order to ensure the prefix influence on the data matches the tail data symbols $\eta = \frac{T_{max}-T_s}{T_s}$ DSS are required after the PFS. Since these symbols are predefined and consistent with every block they may serve the additional function of channel estimation and synchronization.
- Usable Data Symbols: Usable data symbols are separated into two regions. One exists before the PFS, DSS and tail. The other exists in the tail sequence. Since N data symbols will be transmitted in each block, that implies that $\epsilon_2 = \max\{0, \nu - \kappa - \eta\}$ data symbols lie in the tail and $\epsilon_1 = N - \epsilon_2$ data symbols are found before the PFS, DSS, and tail.

One exception should be noted. If $\kappa > (\nu - \eta)$ the tail is simply the DSS preceded by the PFS. In this scenario $\epsilon_2 = 0$ and there is no second PFS and DSS. The prefix size is given by $\rho_{CP} = \max\{\nu, \kappa\}$ Thus, the transmit block efficiency is precisely defined as

$$O_{CP} \triangleq \rho_{CP} + \max\{\nu - \epsilon_2, \kappa\} + \kappa + \eta \quad (4.11)$$

overhead symbols for every N data symbols. This transmission structure is accomplished as in the block diagram of Figure 4.3.

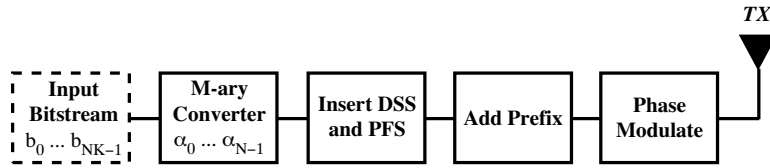


Figure 4.3: Continuous phase transmission block diagram

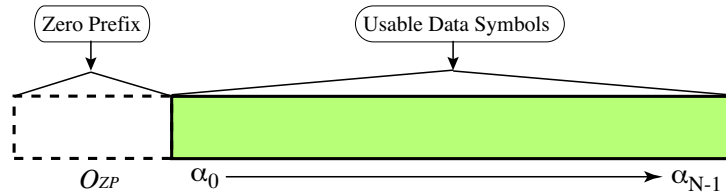


Figure 4.4: Zero prefix data symbol structure

4.0.6.2 Zero Prefix Structure

If we allow ourselves to stop transmitting between data blocks, we can make our data cyclic with less overhead than with the continuous phase structure. The empty symbols between each data block can be sampled. These samples correspond to ISI and partial response of the tail symbols. Thus, by simply adding the zero samples to the beginning of the data block the block is cyclic. The prefix size is $\rho_{ZP} = \max\{\nu, \kappa\}$ giving the transmit block efficiency as

$$O_{ZP} \triangleq \rho_{ZP} \tag{4.12}$$

overhead symbols for every N data symbols. This symbol structure is displayed in Figure 4.4 for transmission as in Figure 4.5.

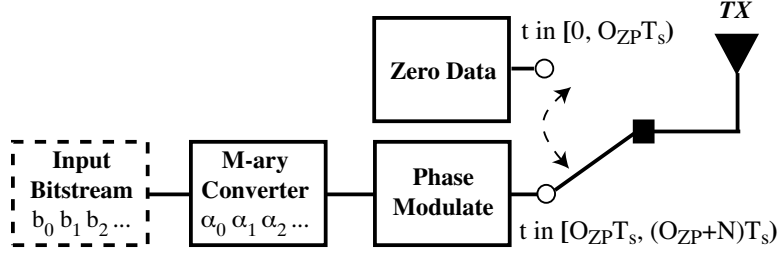


Figure 4.5: Zero prefix transmission block diagram

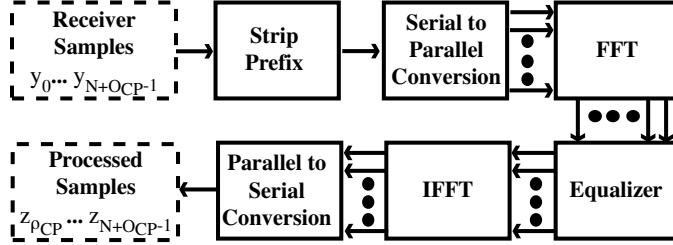


Figure 4.6: FDE components for continuous phase transmission structure

4.0.7 MMSE-LE FDE

Now that the transmission structure has been defined to enable frequency domain equalization, we detail the receiver requirements to enable minimum mean square error (MMSE) equalization. Figure 4.6 and Figure 4.7 show in depth operation of the FDE block in Figure 4.1 for continuous phase and zero prefix transmission structures, respectively. The equalizer input is the discrete Fourier transform of the receiver samples, $y_l[n]$. Recalling (4.5) the DFT of $y_l[n]$ is stated as

$$Y_l[m] = H[m] \tilde{Y}_l[m] + \tilde{V}_l[m] \quad (4.13)$$

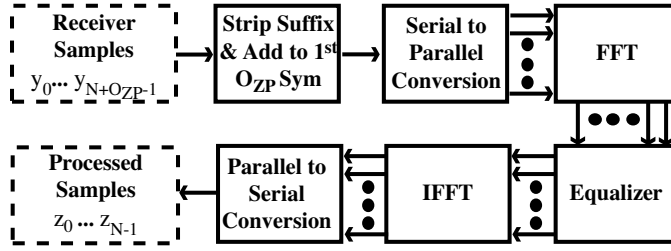


Figure 4.7: FDE components for zero prefix transmission structure

where $H[m]$, $\tilde{Y}_l[m]$, $\tilde{V}_l[m]$ denote the DFT of the frequency selective channel, perfect channel samples, and noise samples respectively. Given this frequency domain description, $Y_l[m]$ we wish to estimate the perfect channel samples, $\tilde{Y}_l[m]$, using a linear equalizer. Therefore we pose the following optimization:

$$G_l[m] = \arg \min_{G'_l[m]} \left\{ \mathbb{E} \left[\left| G'_l[m] Y_l[m] - \tilde{Y}_l[m] \right|^2 \right] \right\} \quad (4.14)$$

where the expectation operation is taken over all possible $\tilde{V}_l[m]$. Unfortunately, this optimization problem cannot be easily solved because the noise term is colored. Before we proceed with our optimization, we must eliminate this correlation structure.

We will precede the MMSE frequency domain filter $G_l[m]$ with a frequency domain whitening filter $W_l[m]$. First, we consider the correlation struc-

ture of the discrete-time noise term $\tilde{v}_l[n]$.

$$\begin{aligned} \mathbb{E} [\tilde{v}_l[n] \tilde{v}_l[n']] &= \int_{nT_s}^{nT_s+T_{max}} \int_{n'T_s}^{n'T_s+T_{max}} \mathbb{E} [v(\tau_1) v^*(\tau_2)] \times \\ &\quad b_l(\tau_1 - nT_s) b_l^*(\tau_2 - n'T_s) d\tau_1 d\tau_2 \end{aligned} \quad (4.15)$$

$$= \sigma^2 \iint_{nT_s}^{n'T_s+T_{max}} b_l(\tau_1 - nT_s) b_l^*(\tau_2 - n'T_s) d\tau_1 d\tau_2 \quad (4.16)$$

$$= \sigma^2 r_{b_l}[n - n'] \quad (4.17)$$

$$= \sigma^2 r_{b_l}[n' - n] \quad (4.18)$$

where we have arbitrarily assumed $n > n'$. Taking the DFT of (4.17) we have

$$DFT \{ \sigma^2 r_{b_l}[n] \} = \sigma^2 R_{b_l}[m]. \quad (4.19)$$

This analysis implies

$$W_l[m] \triangleq \frac{1}{\sqrt{R_{b_l}[m]}} \quad (4.20)$$

such that the sampled noise power spectrum is flat. Given the input $W_l[m] Y_l[m]$ the MMSE equalization analysis is straightforward and can be referenced from [18]. The sought after MMSE linear equalizer in the discrete frequency domain is given as

$$G_l[m] = \frac{W_l^*[m] H^*[m]}{|W_l[m] H[m]|^2 + \frac{1}{SNR}} \quad (4.21)$$

where it should be noted that if we assume, without loss of generality, normalized signal power, then $\frac{1}{SNR} = \sigma^2$.

4.0.8 Complexity Discussion

At first glance the complexity of estimation seems excessive with the multiple matched filter branches and the VA implementation. Indeed, compared to linearly modulated symbols, this CPM detection scheme increases

| R | States | O_{CP} | O_{ZP} |
|-----|--------|----------|----------|
| 1 | 8 | 20 | 20 |
| 2 | 12 | 20 | 20 |
| 3 | 14 | 20 | 20 |
| 4 | 15 | 20 | 20 |

Table 4.1: Complexity comparison for $M = 4$, $L = 2$, $h = \frac{1}{4}$

complexity significantly. In linear modulation receivers a single branch with matched filtering is all that is needed for detection. Furthermore, for full response linearly modulated systems, no VA implementation is necessary (i.e. symbol by symbol detection is optimal for fully equalized signals).

The complexity of the VA is directly related to the number of states to search over. In the implementation due to [12] using the approximate decomposition stated in this report there exist R matched filters. Each matched filter sample is compared to all possible values of $a_l[n]$. The number of possible values of $a_l[n]$ relates directly to the modulation index in (2.3) where the number of states per matched filter, l , equals $\frac{2}{h2^l}$ such that the total states equals $\sum_{l=0}^{R-1} \frac{2}{h2^l}$. Consider, for example, the rectangular pulse functions case when $M = 4$, $L = 2$, and $h = \frac{1}{4}$. We use the approximation with $R = 3$ (the full decomposition has $P = 12$). This essentially optimal (the difference between the approximate and full decomposition is negligible [14]) approximation needs to consider only $8 + 4 + 2 = 14$ states in the VA, making its implementation much more practical. Additionally, for the continuous phase structure $\kappa = 3$, $\eta = 2$, so that for a 10-tap frequency selective channel

($\nu = 10$), only $O_{CP} = 20$ symbols of overhead exist for every N data symbols transmitted. For the zero phase structure $O_{ZP} = 10$. Table 4.1 summarizes the complexity for varying R . In general, this discussion shows that if the approximate decomposition method provides sufficient performance and results in a small number of matched filter branches, we approach a receiver solution sufficient for widespread implementation.

Chapter 5

Conclusion

In this report we have presented a practical method for transmitting power efficient M-ary continuous phase modulation over frequency selective channels. By using frequency domain equalization, a simple and effective method of eliminating intersymbol interference can be accomplished to drastically reduce complexity, making higher order CPM transmissions possible in hostile wireless environments. Equalization for CPM is still a very young area of research and many problems still exist. Notably, effective methods to perform channel estimation and synchronization in frequency selective channels are still unknown.

Bibliography

- [1] J.B. Anderson, T. Aulin, and C-E. Sundberg. *Digital Phase Modulation*. Springer, 1986.
- [2] T. Aulin, N. Rydbeck, and C.-E. Sundberg. Continuous phase modulation—part II: Partial response signaling. *Communications, IEEE Transactions on*, 29(3):210–225, 1981.
- [3] T. Aulin and C. Sundberg. Continuous phase modulation—part i: Full response signaling. *Communications, IEEE Transactions on*, 29(3):196–209, 1981.
- [4] G. Colavolpe and R. Raheli. Reduced-complexity detection and phase synchronization of CPM signals. *IEEE Trans. Commun.*, 45(9):1070–1079, 1997.
- [5] D. Falconer, S.L. Ariyavisitakul, A. Benyamin-Seeyar, and B. Eidson. Frequency domain equalization for single-carrier broadband wireless systems. *IEEE Commun. Mag.*, 40(4):58–66, 2002.
- [6] G. Jr. Forney. Maximum-likelihood sequence estimation of digital sequences in the presence of intersymbol interference. *IEEE Trans. Inform. Theory*, 18(3):363–378, 1972.

- [7] A. Goldsmith. *Wireless Communications*. Cambridge University Press, 2005.
- [8] Kaibin Huang. Supplementary proof for ‘Exact and approximate construction of digital phase modulations by superposition of AMP’ by P. A. Laurent. *IEEE Trans. Commun.*, 53(2):234–237, 2005.
- [9] Xiaojing Huang and Yunxin Li. The PAM decomposition of CPM signals with integer modulation index. *IEEE Trans. Commun.*, 51(4):543–546, 2003.
- [10] J. Huber and W. Liu. An alternative approach to reduced-complexity CPM-receivers. *IEEE J. Select. Areas Commun.*, 7(9):1437–1449, 1989.
- [11] J. Huber and W. Liu. Data-aided synchronization of coherent CPM-receivers. *IEEE Trans. Commun.*, 40(1):178–189, 1992.
- [12] G.K. Kaleh. Simple coherent receivers for partial response continuous phase modulation. *IEEE J. Select. Areas Commun.*, 7(9):1427–1436, 1989.
- [13] P. Laurent. Exact and approximate construction of digital phase modulations by superposition of amplitude modulated pulses (AMP). *Communications, IEEE Transactions on*, 34(2):150–160, 1986.
- [14] U. Mengali and M. Morelli. Decomposition of m-ary CPM signals into PAM waveforms. *IEEE Trans. Inform. Theory*, 41(5):1265–1275, 1995.

- [15] P. Moqvist and T. Aulin. Trellis termination in CPM. *Electronics Letters*, 36(23):1940–1941, 2000.
- [16] F. Pancaldi and G.M. Vitetta. Equalization algorithms in the frequency domain for continuous phase modulations. *IEEE Trans. Commun.*, 54(4):648–658, 2006.
- [17] B.E. Rimoldi. A decomposition approach to CPM. *IEEE Trans. Inform. Theory*, 34(2):260–270, 1988.
- [18] H. Sari, G. Karam, and I. Jeanclaude. Transmission techniques for digital terrestrial TV broadcasting. *IEEE Commun. Mag.*, 33(2):100–109, 1995.
- [19] M.K. Simon. *Bandwidth-Efficient Digital Modulation with Application to Deep-Space Communications*. Wiley-Interscience, 2003.
- [20] M.K. Simon and M.-S. Alouini. *Digital Communication over Fading Channels: A Unified Approach to Performance Analysis*. John Wiley & Sons, Inc., 2000.
- [21] Jun Tan and G.L. Stuber. Frequency-domain equalization for continuous phase modulation. *IEEE Trans. Wireless Commun.*, 4(5):2479–2490, 2005.
- [22] K.C. Yu and A.J. Goldsmith. Linear models and capacity bounds for continuous phase modulation. In *Communications, 2002. ICC 2002. IEEE International Conference on*, volume 2, pages 722–726, 2002.

Vita

Robert Clark Daniels, born in 1980 as the son of Richard and Lynn Daniels, was raised in the rural town of Tunkhannock in northeastern Pennsylvania. He received B.S. degrees (with distinction) in electrical engineering and mathematics from the Pennsylvania State University. Robert is now a member of the Wireless Systems Innovation Laboratory under the direction of Professor Robert W. Heath, Jr. Robert plans to continue his research in pursuit of a Ph.D. in electrical and computer engineering at the University of Texas at Austin. Robert's research interests include implementation issues in wireless systems, large bandwidth wireless personal area networks (including UWB and 60 GHz), and all areas of space-time wireless communications. He is currently working on physical area implementation issues in the upcoming IEEE 802.15.3.c standard.

Permanent address: 504B Nelray Blvd
Austin, Texas 78759

This report was typeset with \LaTeX^\dagger by the author.

[†] \LaTeX is a document preparation system developed by Leslie Lamport as a special version of Donald Knuth's \TeX Program.